

Article

# Exact Solutions of the Bloch Equations of a Two-Level Atom Driven by the Generalized Double Exponential Quotient Pulses with Dephasing

Sofiane Grira <sup>1</sup>, Nadia Boutabba <sup>2,\*</sup> and Hichem Eleuch <sup>3,4</sup>

<sup>1</sup> Department of Applied Sciences and Mathematics, Abu Dhabi University, Abu Dhabi 59911, United Arab Emirates; grira.sofiane@adu.ac.ae

<sup>2</sup> Institute of Applied Technology, Fatima College of Health Sciences, Abu Dhabi 24162, United Arab Emirates

<sup>3</sup> Department of Applied Physics and Astronomy, University of Sharjah, Sharjah 27272, United Arab Emirates; heleuch@sharjah.ac.ae

<sup>4</sup> Institute for Quantum Science and Engineering, Texas A&M University, College Station, TX 77843, USA

\* Correspondence: nadia.boutabba@fchs.ac.ae

**Abstract:** We theoretically investigate a two-level atom driven by a time-dependent external field with a generalized double exponential temporal shape, in the presence of dephasing. Therefore, we provide exact analytical solutions for the population inversion, the real and the imaginary parts of the coherence for a family of chirped and time-dependent laser waveforms. We demonstrate that the remaining atomic population inversion can be controlled by the manipulation of the pulse's shape structure.

**Keywords:** atomic population control; two-level atom; exact solutions

**MSC:** V1V80



**Citation:** Grira, S.; Boutabba, N.; Eleuch, H. Exact Solutions of the Bloch Equations of a Two-Level Atom Driven by the Generalized Double Exponential Quotient Pulses with Dephasing. *Mathematics* **2022**, *10*, 2105. <https://doi.org/10.3390/math10122105>

Academic Editor: Dmitry Makarov

Received: 28 May 2022

Accepted: 14 June 2022

Published: 17 June 2022

**Publisher's Note:** MDPI stays neutral with regard to jurisdictional claims in published maps and institutional affiliations.



**Copyright:** © 2022 by the authors. Licensee MDPI, Basel, Switzerland. This article is an open access article distributed under the terms and conditions of the Creative Commons Attribution (CC BY) license (<https://creativecommons.org/licenses/by/4.0/>).

## 1. Introduction

Bloch equations are commonly used as the foundation framework for modeling the spatial temporal dynamics of diverse mechanisms [1–3]. For instance, they are extensively used to study the dynamics of photo-excited systems [4], the quantum states of spin particles [5] and electron spin nuclear magnetization [6]. Furthermore, they are thoroughly investigated in a range of theoretical and experimental physics [7], either by developing analytical approaches to acquire accurate solutions or by numerical computations [8–10]. Among these approaches, it is worth noting the significance of the non-linear optics experiments (such as NMR) [11,12], the optimal control [13], the magnetization transfer (MT) and the chemical exchange saturation transfer (CEST) [14].

Besides the merits of the computational techniques providing precise numerical solutions for the Bloch equations, the necessity of analytical approaches is crucial. For example, in the field of nuclear magnetic resonance, it was demonstrated that the method of express control [15] is one of the most efficient and preferable. In fact, Davydov et al. [15–18] reported that in order to enhance the information received from the recorded NMR signal, a mathematical model based on accurate analytical solutions of the Bloch equations is required.

As a result, different investigations have emerged to derive the analytical solutions of these coupled equations since 1946 [19,20], immediately after Felix Bloch formulated the Bloch equations to interpret the magnetic resonance phenomena [20]. One noteworthy method was the ab initio solutions provided for various scenarios such as the steady state [21], the on-resonance [22], the zero relaxation [23] and the weak radio-frequency field [24]. Additionally, among other relevant approaches [25–27], one fundamental method was presented in [28], where the authors solved the generalized Bloch equations in the

rotating wave frame by casting the solution into a compact matrix notation as a sum of two terms: one describing the initial state, and the other describing the steady state.

Furthermore, the exact solutions of the Bloch equations for the non-resonant exponential model in the presence of dephasing were given in [29], as were the exact solutions of the Bloch equations for the two-level atom for shaped and chirped pulses with dephasing in [30]. In addition, exact solutions to the Bloch equations for a two-level atom excited by a  $q$ -deformed laser pulse with dephasing and time-dependent detuning were recently presented in [31]. In this situation, the atomic system can be completely controlled by adjusting the asymmetry scaling parameter  $q$  of the  $q$ -deformed hyperbolic laser waveform. Finally, it is worth noting that the time-dependent Bloch equations are solvable using extensive numerical simulations through the application of Laplace transform, the multiple-derivative and the numerical integration method [32–34].

In this work, we derive exact analytical solutions of the Bloch equations describing a two-level atom excited by a laser pulse with the generalized quotient double exponential waveform (Generalized QEXP) for chirped frequencies. Chirping pulses is often utilized in the CPA laser technique [35] (chirped population amplification) to generate ultra-short, high-energy lasers as well as to analyse the high-altitude electromagnetic power (HEMP) [36] and gamma-ray source [37]. These waveforms are extremely efficient when it comes to implementing atomic population transfers in atoms and molecules [38].

This paper is structured as follows: first, we conduct a theoretical analysis to solve the Bloch equations in a two-level atom with dephasing. The considered scheme is driven by the generalized double exponential quotient waveforms under chirped detuning. Next, we report our results, followed by a discussion and concluding remarks. The details are reported in the Appendix A.

## 2. Model

We consider a two-level system (see Figure 1) driven by an external field with internal states  $|1\rangle$  and  $|2\rangle$  and a transition frequency  $\omega$ , where  $\omega = \omega_2 - \omega_1$  and  $\omega_1$  and  $\omega_2$  are the frequencies of the atom at states  $|1\rangle$  and  $|2\rangle$ , respectively. In this case, the Hamiltonian is written in terms of the Pauli matrices  $\sigma_x$ , and  $\sigma_z$  and the time-dependent driving field  $\Omega(t)$  as:

$$H = \frac{\hbar}{2} (\Delta(t)\sigma_z + \Omega(t)\sigma_x) \quad (1)$$

where the Rabi frequency is proportional to the amplitude of the laser pulse as:

$$\Omega(t) = -d \frac{E(t)}{\hbar} \quad (2)$$

here,  $d$  denotes the dipole moment;  $\Delta = \omega_2 - \omega_1$  is the time-dependent detuning. The master equation that governs the systems dynamics is given by the density matrix evolution as:

$$\frac{d\rho(t)}{dt} = -i[H, \rho] + \frac{\Gamma}{2} (\sigma_z \rho \sigma_z - \rho) \quad (3)$$

where the dephasing rate is given by  $\Gamma$  and it is inversely proportional to the decoherence time. It is worth noting that the total Hamiltonian is the sum of the field-free Hamiltonian and the interaction of the atom with the electromagnetic fields. This is basically written in terms of the annihilation and creation operators; full details can be found in [39]. In addition, the first part of the density matrix evolution describes the free evolution of the system, and the second part represents the system evolution as a result of decoherence connected to the dephasing rate.

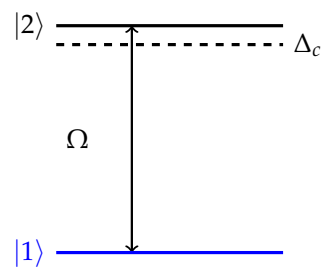


Figure 1. Two-level atom.

The goal of this research is to derive exact analytical solutions of the density matrix elements in order to determine the atomic population inversion  $w = \rho_{22} - \rho_{11}$  at the steady state ( $t = \infty$ ). The two-level atom studied is excited by a shaped laser and it takes place under a chirped detuning.

The time evolution of atomic populations and coherences are given in terms of the Bloch equations by [40]:

$$\begin{bmatrix} \frac{du(t)}{dt} \\ \frac{dv(t)}{dt} \\ \frac{dw(t)}{dt} \end{bmatrix} = \begin{bmatrix} -\Gamma & -\Delta(t) & 0 \\ \Delta(t) & -\Gamma & -\Omega(t) \\ 0 & \Omega(t) & 0 \end{bmatrix} \begin{bmatrix} u(t) \\ v(t) \\ w(t) \end{bmatrix} \tag{4}$$

Here, the atomic population inversion between the higher state  $|2\rangle$  and the ground state  $|1\rangle$  is denoted by  $w = \rho_{22} - \rho_{11}$ , whereas  $u(t)$  and  $v(t)$  represent the real and the imaginary part of the atom-field coherence  $\rho_{12}(t)$ .

### 3. Exact Solutions: The Generalized QEXP Pulses

The aim of this section is to establish exact analytical solutions for the atomic population and the coherence of the following optical pulse shape:

$$\Omega = \sqrt{\frac{\alpha}{1-\alpha}} \frac{A_1 \Gamma e^{-3\Gamma t}}{\left( K e^{-2\Gamma t} + \frac{1-\alpha}{\alpha} \right)^{\frac{3}{2}}} \tag{5}$$

under chirped detuning of the form:

$$\Delta = \frac{K \Gamma e^{-2\Gamma t}}{\left( K e^{-2\Gamma t} + \frac{1-\alpha}{\alpha} \right)^{\frac{3}{2}}} \tag{6}$$

where  $A_1, K$  are positive constants and  $0 < \alpha < 1$ .  $A_1$  is related to the amplitude of the pulse, whereas  $K$  is a parameter related to the pulse shape. In order to solve the Bloch equations (Equation (4)), we introduce three new variables:  $v_1, u_1$  and  $w_1$  related to the previous variables  $u(t), v(t)$  and  $w(t)$  as:

$$v_1(t) = v(t)e^{\Gamma t} \tag{7}$$

$$u_1(t) = u(t)e^{\Gamma t} \tag{8}$$

$$w_1(t) = w(t)e^{\Gamma t} \tag{9}$$

in addition, by using new change of variables  $x = \int \Delta(t)dt$ , and considering  $g(x) = \frac{\Omega(x)}{\Delta(x)}$  and  $h(x) = \frac{\Gamma}{\Delta(x)}$ , Equation (4) gives:

$$\frac{du_1}{dx} = -v_1(x) \tag{10}$$

$$\frac{dv_1}{dx} = u_1(x) - g(x)w_1(x) \tag{11}$$

$$\frac{dw_1}{dx} = h(x)w_1(x) + g(x)v_1(x) \tag{12}$$

This system of differential equations will serve as a basis for our future analysis to establish the exact solutions for the considered pulse. The variable  $x(t)$  is defined as:

$$x(t) = \frac{1}{\sqrt{Ke^{-2\Gamma t} + \frac{1-\alpha}{\alpha}}}$$

We obtain linear second- and third-order ordinary differential equations through repetitive differentiation and substitution of the Equations (10)–(12).

$$\frac{d^3u_1}{dx^3} + \frac{\alpha}{(1-\alpha)x^2} \frac{du_1}{dx} = 0 \tag{13}$$

$$\frac{d^2v_1}{dx^2} + \frac{\alpha}{(1-\alpha)x^2} \frac{dv_1}{dx} = 0 \tag{14}$$

$$\begin{aligned} \frac{d^3w_1}{dx^3} + \frac{\alpha}{\alpha x + (\alpha - 1)x^3} \frac{d^2w_1}{dx^2} - \left( \frac{(x^4 + 5x^2 + 1)\alpha^3 - (2x^4 + 8x^2)\alpha^2 + \alpha x^4 + 3\alpha x^2}{x^2(\alpha x^2 - x^2 + \alpha)^2(\alpha - 1)} \right) \frac{dw_1}{dx} + \\ \left( \frac{(-11x^4 + 5x^2 + 1)\alpha^4 + (34x^4 - 8x^2)\alpha^3 + (3x^2 - 35x^4)\alpha^2 + 12\alpha x^4}{x^3(\alpha x^2 - x^2 + \alpha)^3(\alpha - 1)} \right) w_1 = 0 \end{aligned} \tag{15}$$

Equation (13) is the Cauchy–Euler equation. Thus,  $y = x^m$  is a solution of the differential equation whenever  $m$  is a solution of the auxiliary equation

$$m \left( m^2 - 3m + \frac{2 - \alpha}{1 - \alpha} \right) = 0$$

There are three different cases to be considered, depending on whether the roots of this auxiliary equation are real and distinct ( $0 < \alpha < \frac{1}{5}$ ), real and equal ( $\alpha = \frac{1}{5}$ ), or complex ( $\frac{1}{5} < \alpha < 1$ ).

Solving the last equation leads to three different solutions  $u_1(t)$ ,  $v_1(t)$  and  $w_1$  according to the domain of  $\alpha$ . As a result, the exact solutions of coherence and population inversion can be derived. We consider  $u(0) = 0$ ,  $v(0) = 0$ ,  $w(0) = -1$  as initial conditions of the two-level system (which means that the initial population is in the ground state). By following the above steps, our methods allow us to obtain two families of dynamical solutions: the solutions in the case  $0 < \alpha < \frac{1}{5}$  and  $\frac{1}{5} < \alpha < 1$ . All details are given in the Appendix A. The case  $\alpha = \frac{1}{5}$  is irrelevant for the study of Atomic Population Inversion, since it is a constant.

#### 4. Discussion

By analytically solving Equation (13), we get a spectrum of solutions that depends on  $\alpha$ . Therefore, in this part, we discuss the atomic population inversion at the steady state (infinity) for the obtained solutions for two different cases:  $0 < \alpha < \frac{1}{5}$  and  $\frac{1}{5} < \alpha < 1$ . Hence, we first start examining the case  $\frac{1}{5} < \alpha < 1$ . For  $\alpha$  equals to  $\frac{1}{2}$ , we notice that Equation (13) becomes:

$$\frac{d^3u_1}{dx^3} + \frac{1}{x^2} \frac{du_1}{dx} = 0 \tag{16}$$

This is generated by leads the Modified QEXP pulse analyzed in [41], where the pulse form is given by:

$$\Omega(t) = \frac{\Omega_c e^{-3\Gamma t}}{(1 + e^{-2\Gamma t})^{\frac{3}{2}}} \tag{17}$$

For this specific case, the form of the pulse is plotted in Figure 2a. Here, we plot the normalized pulse. In fact, we can write  $\Omega(t) = \frac{\Gamma}{k}f(t)$ , where

$$f(t) = k\Omega(t) \tag{18}$$

and  $k$  is a factor of normalization to impose  $f_{max} = 1$ , as mentioned in [42]. Here,  $\Gamma$  is a scaling variable inversely proportional to the atom life time;  $t$  is in the pulse rise time units denoted by  $\tau$ . Notably, for a Multi-Level atom,  $\tau$  is related to the atom lifetime. The relation between the pulse width, the rabi frequency scaling factor and the atomic system such as the Rubidium atom is detailed in [43].  $\Omega_c$  is the Rabi frequency utilized in the two-level atom model, and the fall edge of  $f(t)$  is governed by the exponential powers. Different pulses with the mathematical description of exponential and modified exponential waveforms are discussed in [42], where all possible realistic parameters and their practical realization are listed in Table II of [42].

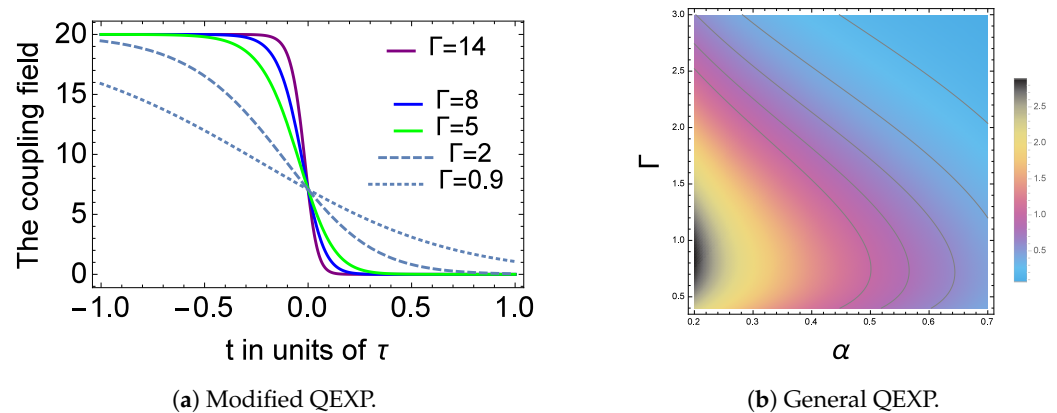


**Figure 2.** The QEXP waveforms: (a) The modified QEXP pulse dynamics for various pulse rise time factors  $\Gamma$ . (b) The Generalized QEXP pulse dynamics in terms of the shape factor  $\alpha$  and the pulse rise time  $\Gamma$ .

For  $\alpha$  different from  $\frac{1}{2}$ , Equation (13) leads to a Generalized QEXP pulse with a form given by:

$$\Omega(t) = \sqrt{n}^{-1} A_1 \Gamma e^{-3\Gamma t} ((n + Ke^{-2\Gamma t}))^{-\frac{1}{2}} \tag{19}$$

where  $n = \frac{\alpha}{1-\alpha}$ . The form of the pulse is plotted in Figure 2b.

Finally, we discuss the atomic population inversion at the steady state for the obtained solutions at both cases. First, for the case  $0 < \alpha < \frac{1}{5}$ , the stationary solution reads:

$$w(\infty) = \frac{1}{(2\alpha - 4)\sqrt{5\alpha^2 - 6\alpha + 1}} \left[ (1 - \alpha)(a_\alpha - 1) \left(\frac{1}{1 - \alpha}\right)^{\bar{a}_\alpha + 1} - \right. \tag{20}$$

$$3\alpha(\alpha - 1) \left(\alpha - \frac{1}{3}\sqrt{5\alpha^2 - 6\alpha + 1} - 1\right) \left(\frac{1}{1 - \alpha}\right)^{\frac{1}{2}\bar{b}_\alpha} +$$

$$3\alpha(\alpha - 1) \left(\alpha + \frac{1}{3}\sqrt{5\alpha^2 - 6\alpha + 1} - 1\right) \left(\frac{1}{1 - \alpha}\right)^{\frac{1}{2}b_\alpha} +$$

$$\left. (\alpha - 1)(\bar{a}_\alpha - 1) \left(\frac{1}{1 - \alpha}\right)^{\frac{1}{2}b_\alpha + 1} - 2\alpha(\alpha - 1)\sqrt{5\alpha^2 - 6\alpha + 1} \right]$$

where

$$a_\alpha = \frac{1}{-2 + 2\alpha} \left( 3\alpha - 3 + \sqrt{5\alpha^2 - 6\alpha + 1} \right), \tag{21}$$

$$b_\alpha = \frac{1}{-2 + 2\alpha} \left( -3\alpha + 3 + \sqrt{5\alpha^2 - 6\alpha + 1} \right), \tag{22}$$

$$\bar{a}_\alpha = \frac{1}{-2 + 2\alpha} \left( 3\alpha - 3 - \sqrt{5\alpha^2 - 6\alpha + 1} \right), \tag{23}$$

and

$$\bar{b}_\alpha = \frac{1}{-2 + 2\alpha} \left( -3\alpha + 3 - \sqrt{5\alpha^2 - 6\alpha + 1} \right). \tag{24}$$

For this family of pulses (see Figure 3a), the variation of the parameter  $\alpha$  in the interval  $(0, 0.2)$  has no effect on the population inversion at the steady state. We also notice that the remaining population is proportional to the initial population at the ground state. If we consider the following initial conditions  $u(0) = 2\sqrt{A(1-A)}$ ,  $v(0) = 0$ ,  $w(0) = 1 - 2A$  where  $0 \leq A \leq 1$ , then we can highlight three crucial points: (1) for  $A = 1$ , the considered initial population is in the ground state and the population left at the steady state is also in the ground state. (2) For  $A = 0.5$ , the population in the ground and the excited states are the same whereas, the population inversion is almost vanishing. (3) For  $A = 0$ , the total population is initially in the excited state and for this specific condition, we get a total inversion of the remaining population. In addition, we note that the population inversion is almost insensitive to the structure of the shape. For the case  $\frac{1}{5} < \alpha < 1$ , the stationary solution is:

$$w(\infty) = \frac{1 - \alpha}{(\alpha - 2)\sqrt{-5\alpha^2 + 6\alpha - 1}} \left[ 2(1 + \alpha)(1 - \alpha)^{\frac{1}{4}} \sin r_\alpha + 2(1 - \alpha)^{\frac{1}{4}} \sqrt{-5\alpha^2 + 6\alpha - 1} \cos r_\alpha + \alpha \sqrt{-5\alpha^2 + 6\alpha - 1} \right] \tag{25}$$

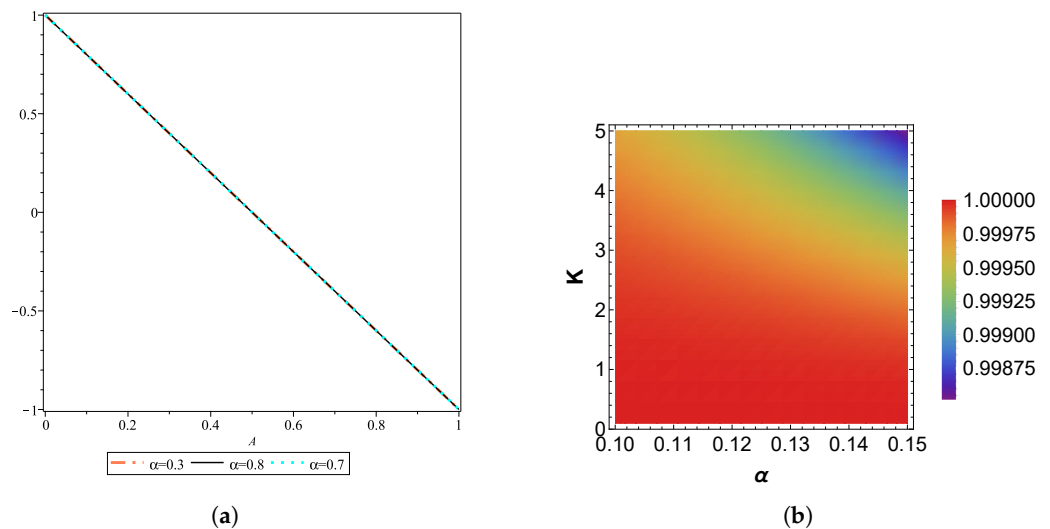


**Figure 3.** (a) Atomic population inversion left at the steady state in terms of the initial populations for  $A_1 = 1, K = 1$  and  $0 < \alpha < \frac{1}{5}$ ; (b) atomic population inversion left at the steady state in terms of the shape factor  $\alpha$  and the deformation factor  $K$ , where  $A_1 = \sqrt{K^3}$  for  $0 < \alpha < \frac{1}{5}$ .

In contrast with the previous case (very small  $\alpha$ ), we observe (in Figure 4) that the population inversion is sensitive to the parameter  $\alpha$ , which represents the shape of the pulse.  $\alpha$  is relatively large in  $(0.2, 1)$ . With rising  $\alpha$ , the population left in the excited state is no longer linear as a function of the initial population of the ground state. Hence, we highlight three significant cases: (1) For  $(A = 1)$ , the initial population is in the ground state, and the population left at the steady state is highly dependent on  $\alpha$ . For a critical value of  $\alpha_c = 0.79696565$ , we get zero inversion of population.

For  $\rho_{11} = \rho_{22}$  at steady state = 0.5, we obtain a population inversion above this critical value of  $\alpha_c$ . (2) For the case of a coherent superposition ( $A = 0.5$ ), raising the parameter  $\alpha$  enhances the population inversion over long time-scales. (3) For the case where the total population is initially in the excited state ( $A = 0$ ), an increase of  $\alpha$  leads to a reduction of the population left at the excited state. Hence, we can conclude that the shape of the

pulse controls the distribution of the remaining population. This can be seen in both Figures 3b and 4b, where we can vary both the shape factor  $\alpha$  (that is, the amplitude of the rabi frequency) and the deformation factor  $K$ . In both figures, we notice that the atomic population inversion at the steady state is in general more sensitive to the shape effect than the deformation. In order to clearly see the temporal dynamics of the input pulse with both variable amplitude and variable deformation, we include Figure A1 in the Appendix A. Finally, we believe that our analytical solution of the Bloch equations for a wide spectrum of shaped waveforms (the Generalized QEXP pulse in terms of shape factor  $\alpha$ ), is of great interest to the NMR field. In fact, and to the best of our knowledge, few analytical solutions are currently available. For instance, the authors in [44] have derived solutions of the Bloch equations for the hyperbolic secant function and they have reported pertinent results, including the influence of the magnetization in the studied case by changing the pulse parameters.

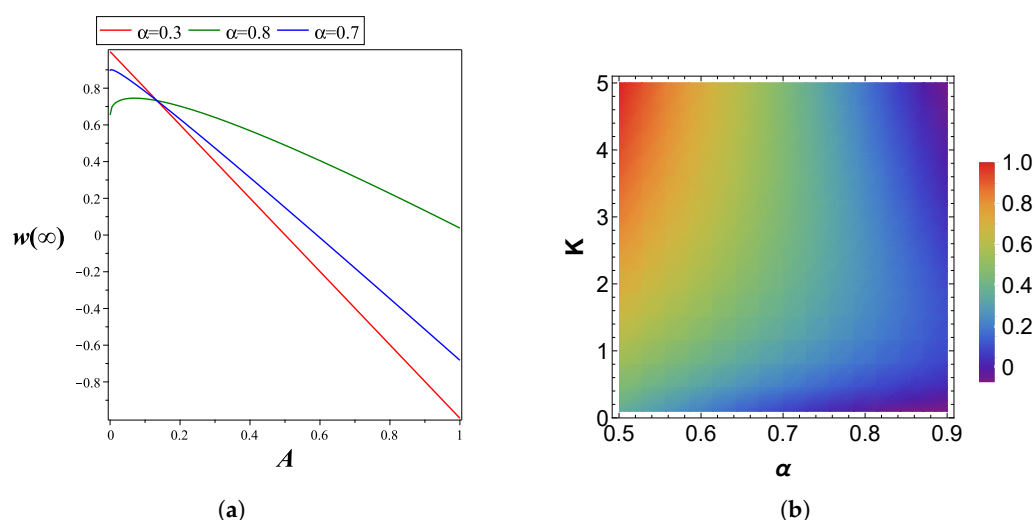


**Figure 4.** (a) Atomic population inversion left at the steady state in terms of the initial populations for  $A_1 = 1$ ,  $K = 1$  and  $\frac{1}{5} < \alpha < 1$ ; (b) atomic population inversion left at the steady state in terms of the shape factor  $\alpha$  and the deformation factor  $K$ , where  $A = \sqrt{K^3}$  for  $\frac{1}{5} < \alpha < 1$ .

## 5. Conclusions

In this study, we have explored the effect of the generalized double exponential waveform on a two-level atom with dephasing. By solving the Bloch equations for chirped detuning and shaped pulses, we get the exact analytical solutions of both the atomic population and the coherence. Hence, the stationary atomic population inversion is discussed in terms of the shape structure of the pulse. We report that for typical values of the shape structure, the atomic population inversion can be enhanced for different initial distributions of the atomic population between the ground and the excited states. Such analytical solutions of the Bloch equations for specific pulse shaping might be useful in the NMR field.

**Author Contributions:** Investigation, S.G., N.B. and H.E. All authors have read and agreed to the published version of the manuscript.

**Funding:** This research received no external funding.

**Institutional Review Board Statement:** Not applicable.

**Informed Consent Statement:** Not applicable.

**Data Availability Statement:** Not applicable.

**Conflicts of Interest:** The authors declare no conflict of interest.

**Appendix A**

Appendix A.1. Case 1:  $0 < \alpha < \frac{1}{5}$

Let

$$a_\alpha = \frac{1}{-2 + 2\alpha} \left( 3\alpha - 3 + \sqrt{5\alpha^2 - 6\alpha + 1} \right), \tag{A1}$$

$$b_\alpha = \frac{1}{-2 + 2\alpha} \left( -3\alpha + 3 + \sqrt{5\alpha^2 - 6\alpha + 1} \right), \tag{A2}$$

$$\bar{a}_\alpha = \frac{1}{-2 + 2\alpha} \left( 3\alpha - 3 - \sqrt{5\alpha^2 - 6\alpha + 1} \right), \tag{A3}$$

and

$$K_{\alpha,t} = \alpha e^{-2t} - \alpha + 1$$

Then, the solution of Equation (13) is

$$u_1(x) = c_1 + c_2 x^{a_\alpha} + c_3 x^{-b_\alpha} \tag{A4}$$

and we deduct from the above system of differential equations

$$v_1(x) = \frac{-c_2 a_\alpha}{(-2 + 2\alpha)x} x^{a_\alpha} + \frac{c_3 b_\alpha}{(-2 + 2\alpha)x} x^{-b_\alpha} \tag{A5}$$

where

$$c_1 = \frac{-\alpha(\alpha - 1)}{\alpha - 2},$$

$$c_2 = \frac{\alpha^{\frac{\alpha-1-\sqrt{5\alpha^2-6\alpha+1}}{4\alpha-4}} b_\alpha (\alpha - 1)^2}{(\alpha - 2)\sqrt{5\alpha^2 - 6\alpha + 1}},$$

and

$$c_3 = \frac{\alpha^{\frac{\alpha-1+\sqrt{5\alpha^2-6\alpha+1}}{4\alpha-4}} a_\alpha (\alpha - 1)^2}{(\alpha - 2)\sqrt{5\alpha^2 - 6\alpha + 1}}$$

Consequently, the expressions of the real and imaginary parts of the coherence are given by:

$$u(t) = \left[ c_1 + c_2 \left( Ke^{-2\Gamma t} + \frac{1-\alpha}{\alpha} \right)^{-\frac{a_\alpha}{2}} + c_3 \left( Ke^{-2\Gamma t} + \frac{1-\alpha}{\alpha} \right)^{\frac{b_\alpha}{2}} \right] e^{-\Gamma t} \tag{A6}$$

$$v(t) = \left[ \frac{-c_2 a_\alpha}{(-2 + 2\alpha)} \left( Ke^{-2\Gamma t} + \frac{1-\alpha}{\alpha} \right)^{\frac{1-a_\alpha}{2}} + \frac{c_3 b_\alpha}{(-2 + 2\alpha)} \left( Ke^{-2\Gamma t} + \frac{1-\alpha}{\alpha} \right)^{\frac{1+b_\alpha}{2}} \right] e^{-\Gamma t} \tag{A7}$$

For  $K = 1$ , we get the dynamics of the atomic population inversion:

$$w(t) = \frac{1}{(2\alpha - 4)\sqrt{5\alpha^2 - 6\alpha + 1}} \left[ (1 - \alpha)(a_\alpha - 1)K_{\alpha,t}^{\bar{a}_\alpha+1} - 3\alpha(\alpha - 1)\left(\alpha - \frac{1}{3}\sqrt{5\alpha^2 - 6\alpha + 1} - 1\right)K_{\alpha,t}^{\frac{1}{2}\bar{b}_\alpha} + 3\alpha(\alpha - 1)\left(\alpha + \frac{1}{3}\sqrt{5\alpha^2 - 6\alpha + 1} - 1\right)K_{\alpha,t}^{\frac{1}{2}b_\alpha} + (\alpha - 1)(\bar{a}_\alpha - 1)K_{\alpha,t}^{\frac{1}{2}\bar{b}_\alpha+1} - 2\alpha(\alpha - 1)\sqrt{5\alpha^2 - 6\alpha + 1} \right] \tag{A8}$$

At the steady state, we get:

$$\begin{aligned}
 w(\infty) = & \frac{1}{(2\alpha - 4)\sqrt{5\alpha^2 - 6\alpha + 1}} \left[ (1 - \alpha)(a_\alpha - 1) \left( \frac{1}{1 - \alpha} \right)^{\bar{a}_\alpha + 1} - \right. & (A9) \\
 & 3\alpha(\alpha - 1) \left( \alpha - \frac{1}{3}\sqrt{5\alpha^2 - 6\alpha + 1} - 1 \right) \left( \frac{1}{1 - \alpha} \right)^{\frac{1}{2}\bar{b}_\alpha} + \\
 & 3\alpha(\alpha - 1) \left( \alpha + \frac{1}{3}\sqrt{5\alpha^2 - 6\alpha + 1} - 1 \right) \left( \frac{1}{1 - \alpha} \right)^{\frac{1}{2}b_\alpha} + \\
 & \left. (\alpha - 1)(\bar{a}_\alpha - 1) \left( \frac{1}{1 - \alpha} \right)^{\frac{1}{2}b_\alpha + 1} - 2\alpha(\alpha - 1)\sqrt{5\alpha^2 - 6\alpha + 1} \right]
 \end{aligned}$$

Appendix A.2. Case 2:  $\frac{1}{5} < \alpha < 1$

We note that in this case, the pulse shape is reported in (Figure A1), where the General Qexp waveform depends on different  $\alpha$  and  $\frac{1}{5} < \alpha < 1$ .

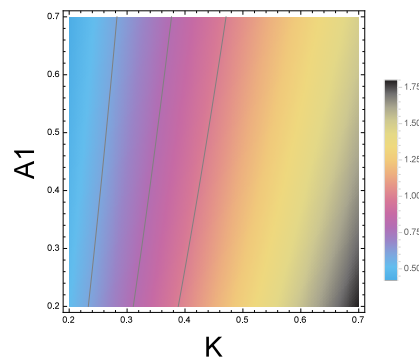


**Figure A1.** The generalized QEXP pulse dynamics for various amplitudes  $A_1$  and different deformations  $K$ .

Let

$$e_\alpha = \frac{\sqrt{-5\alpha^2 + 6\alpha - 1}}{-2 + 2\alpha}$$

Then, the solution of Equation (13) is

$$u_1(x) = c_1 + c_2 x^{\frac{3}{2}} \sin(e_\alpha \ln x) + c_3 x^{\frac{3}{2}} \cos(e_\alpha \ln x) \tag{A10}$$

and

$$v_1(x) = -\frac{3}{2}c_2 \sqrt{x} \sin(e_\alpha \ln x) - \frac{c_2 \sqrt{x} \sqrt{-5\alpha^2 + 6\alpha - 1} \cos(e_\alpha \ln x)}{-2 + 2\alpha} - \tag{A11}$$

$$\frac{3}{2}c_3 \sqrt{x} \cos(e_\alpha \ln x) + \frac{c_3 \sqrt{x} \sqrt{-5\alpha^2 + 6\alpha - 1} \sin(e_\alpha \ln x)}{-2 + 2\alpha} \tag{A12}$$

where

$$c_1 = -\frac{\alpha(\alpha - 1)}{\alpha - 2},$$

$$c_2 = -\frac{3\alpha^{\frac{1}{4}}(\alpha - 1) \left( (\alpha - 1) \cos\left(\frac{e_\alpha \ln \alpha}{2}\right) - \frac{1}{3}\sqrt{-5\alpha^2 + 6\alpha - 1} \sin\left(\frac{e_\alpha \ln \alpha}{2}\right) \right)}{\sqrt{-5\alpha^2 + 6\alpha - 1}(\alpha - 2)}$$

and

$$c_3 = \frac{\alpha^{\frac{1}{4}}(\alpha - 1) \left( \sqrt{-5\alpha^2 + 6\alpha - 1} \cos\left(\frac{e_\alpha}{2} \ln \alpha\right) + 3(\alpha - 1) \sin\left(\frac{e_\alpha}{2} \ln \alpha\right) \right)}{\sqrt{-5\alpha^2 + 6\alpha - 1}(\alpha - 2)}$$

Let

$$t_\alpha = \frac{\sqrt{-5\alpha^2 + 6\alpha - 1} \ln(\alpha e^{-2t} - \alpha + 1)}{-4 + 4\alpha}$$

The real part of the coherence is:

$$u(t) = \frac{1}{\sqrt{-5\alpha^2 + 6\alpha - 1}(\alpha e^{-2t} - \alpha + 1)^{\frac{3}{4}}(\alpha - 2)} \left[ (3\alpha - 3) \sin t_\alpha + \right. \tag{A13}$$

$$\left. \sqrt{-5\alpha^2 + 6\alpha - 1} \left( \cos t_\alpha - (\alpha e^{-2t} - \alpha + 1)^{\frac{3}{4}} \right) \alpha(\alpha - 1)e^{-t} \right] \tag{A14}$$

In addition, the imaginary part of the coherence is:

$$v(t) = - \frac{2e^{-t} \alpha^{\frac{1}{4}}(\alpha - 1)}{\sqrt{-5\alpha^2 + 6\alpha - 1} \left( \frac{\alpha e^{-2t} - \alpha + 1}{\alpha} \right)^{\frac{1}{4}}} \sin t_\alpha \tag{A15}$$

Finally, the atomic population inversion is:

$$w(t) = - \frac{1}{\sqrt{-5\alpha^2 + 6\alpha - 1}(\alpha e^{-2t} - \alpha + 1)(\alpha - 2)} \left[ (1 - \alpha)(\alpha e^{-2t} - \alpha + 1)^{\frac{1}{4}}((\alpha^2 - 2\alpha)e^{-2t} + 2\alpha^2 - 2) \sin t_\alpha + \right. \\ \left. \sqrt{-5\alpha^2 + 6\alpha - 1} \left( (\alpha e^{-2t} - \alpha + 1)^{\frac{1}{4}}((\alpha^2 - 2\alpha)e^{-2t} - 2(\alpha - 1)^2) \cos t_\alpha + \right. \right. \\ \left. \left. \alpha(\alpha - 1)(\alpha e^{-2t} - \alpha + 1) \right) \right]$$

$$w(\infty) = \frac{1 - \alpha}{(\alpha - 2)\sqrt{-5\alpha^2 + 6\alpha - 1}} \left[ 2(1 + \alpha)(1 - \alpha)^{\frac{1}{4}} \sin r_\alpha + \right. \tag{A16} \\ \left. 2(1 - \alpha)^{\frac{1}{4}} \sqrt{-5\alpha^2 + 6\alpha - 1} \cos r_\alpha + \alpha \sqrt{-5\alpha^2 + 6\alpha - 1} \right]$$

where

$$r_\alpha = \frac{\sqrt{-5\alpha^2 + 6\alpha - 1} \ln(1 - \alpha)}{-4 + 4\alpha}$$

Appendix A.3. Case 3:  $\alpha = \frac{1}{5}$

Let

$$c_1 = -\frac{4}{45},$$

$$c_2 = \frac{2 \left( 3 \ln\left(\frac{\sqrt{5}}{5}\right) + 2 \right) 5^{\frac{3}{4}}}{45}$$

$$c_3 = -\frac{25^{\frac{3}{4}}}{15}$$

Then, the solution of Equation (13) is

$$u_1(x) = c_1 + c_2 x^{\frac{3}{2}} + c_3 x^{\frac{3}{2}} \ln(x) \tag{A17}$$

and we get

$$v_1(x) = -\frac{3}{2}c_2\sqrt{x} - \frac{3}{2}c_3\sqrt{x}\ln(x) - c_3\sqrt{x} \quad (\text{A18})$$

Consequently, the expressions of the real and imaginary parts of the coherence are given by:

$$u(t) = \left[ c_1 + c_2 \left( Ke^{-2\Gamma t} + 4 \right)^{-\frac{3}{4}} - \frac{1}{2}c_3 \ln(Ke^{-2\Gamma t} + 4) \left( Ke^{-2\Gamma t} + 4 \right)^{-\frac{3}{4}} \right] e^{-\Gamma t} \quad (\text{A19})$$

$$v(t) = \left[ -\frac{3}{2}c_2 \left( Ke^{-2\Gamma t} + 4 \right)^{-\frac{1}{4}} + \frac{3}{4}c_3 \ln(Ke^{-2\Gamma t} + 4) \left( Ke^{-2\Gamma t} + 4 \right)^{-\frac{3}{4}} - c_3 \left( Ke^{-2\Gamma t} + 4 \right)^{-\frac{1}{4}} \right] e^{-\Gamma t} \quad (\text{A20})$$

$$\begin{aligned} w(t) = & c_1 + c_2 \left( Ke^{-2\Gamma t} + 4 \right)^{-\frac{3}{4}} - \frac{1}{2}c_3 \ln(Ke^{-2\Gamma t} + 4) \left( Ke^{-2\Gamma t} + 4 \right)^{-\frac{3}{4}} + \\ & \frac{3}{4}c_2 \left( Ke^{-2\Gamma t} + 4 \right)^{\frac{1}{4}} - \frac{3}{8}c_3 \ln(Ke^{-2\Gamma t} + 4) \left( Ke^{-2\Gamma t} + 4 \right)^{\frac{1}{4}} + \\ & 2c_3 \left( Ke^{-2\Gamma t} + 4 \right)^{\frac{1}{4}} \end{aligned} \quad (\text{A21})$$

## References

1. Wilhelm, J.; Grössing, P.; Seith, A.; Crewse, J.; Nitsch, M.; Weigl, L.; Schmid, C.; Evers, F. Semiconductor Bloch-equations formalism: Derivation and application to high-harmonic generation from Dirac fermions. *Phys. Rev. B* **2021**, *103*, 125419. [\[CrossRef\]](#)
2. Friedberg, R.; Manassah, J.T. Solutions of the Maxwell–Bloch equations in (1, 1)-d in the presence of a pulsed pump. *Opt. Commun.* **2021**, *501*, 127389. [\[CrossRef\]](#)
3. Davydov, M.; Davydov, V.; Rud, V.Y. On necessity for analytical solution of the Bloch equations for nuclear magnetic resonance signals at condition express control of liquid medium. *J. Phys. Conf. Ser.* **2021**, *2086*, 012134. [\[CrossRef\]](#)
4. Cao, B.; Grass, T.; Gazzano, O.; Patel, K.A.; Hu, J.; Müller, M.; Huber, T.; Anzi, L.; Watanabe, K.; Taniguchi, T.; et al. Chiral transport of hot carriers in graphene in the quantum Hall regime. *arXiv* **2021**, arXiv:2110.01079.
5. Torrey, H.C. Bloch equations with diffusion terms. *Phys. Rev.* **1956**, *104*, 563. [\[CrossRef\]](#)
6. Vlassenbroek, A.; Jeener, J.; Broekaert, P. Macroscopic and microscopic fields in high-resolution liquid NMR. *J. Magn. Reson. Ser. A* **1996**, *118*, 234–246. [\[CrossRef\]](#)
7. Foklin, J.; Tarbutt, M. Laser cooling and magneto-optical trapping of molecules analyzed using optical Bloch equations and the Fokker-Planck-Kramers equation. *Phys. Rev. A* **2018**, *98*, 063415. [\[CrossRef\]](#)
8. Ben-Eliezer, N.; Sodickson, D.K.; Block, K.T. Rapid and accurate T2 mapping from multi-spin-echo data using Bloch-simulation-based reconstruction. *Magn. Reson. Med.* **2015**, *73*, 809–817. [\[CrossRef\]](#)
9. Singh, H.; Singh, C. A reliable method based on second kind Chebyshev polynomial for the fractional model of Bloch equation. *Alex. Eng. J.* **2018**, *57*, 1425–1432. [\[CrossRef\]](#)
10. Jurczuk, K.; Kretowski, M.; Bellanger, J.J.; Eliat, P.A.; Saint-Jalmes, H.; Bézy-Wendling, J. Computational modeling of MR flow imaging by the lattice Boltzmann method and Bloch equation. *Magn. Reson. Imaging* **2013**, *31*, 1163–1173. [\[CrossRef\]](#)
11. Guenther, C.; Amthor, T.; Doneva, M.; Kozerke, S. A unifying view on extended phase graphs and Bloch simulations for quantitative MRI. *Sci. Rep.* **2021**, *11*, 21289. [\[CrossRef\]](#) [\[PubMed\]](#)
12. Telkki, V.V.; Urbańczyk, M.; Zhivonitko, V. Ultrafast methods for relaxation and diffusion. *Prog. Nucl. Magn. Reson. Spectrosc.* **2021**, *126*, 101–120. [\[CrossRef\]](#) [\[PubMed\]](#)
13. Sango-Solanas, P.; Tse Ve Koon, K.; Van Reeth, E.; Ratiney, H.; Millioz, F.; Caussy, C.; Beuf, O. Short echo time dual-frequency MR Elastography with Optimal Control RF pulses. *Sci. Rep.* **2022**, *12*, 1406. [\[CrossRef\]](#) [\[PubMed\]](#)
14. Assländer, J.; Gultekin, C.; Flassbeck, S.; Glaser, S.J.; Sodickson, D.K. Generalized Bloch model: A theory for pulsed magnetization transfer. *Magn. Reson. Med.* **2022**, *87*, 2003–2017. [\[CrossRef\]](#)
15. Davydov, V.; Dudkin, V.; Vysoczky, M.; Myazin, N. Small-size NMR spectrometer for express control of liquid media state. *Appl. Magn. Reson.* **2020**, *51*, 653–666. [\[CrossRef\]](#)
16. Myazin, N.; Davydov, V.; Rud, V.Y.; Yushkova, V.; Dudkin, V. New method for determining the composition of liquid media during the express control of their state using the nuclear magnetic resonance phenomena. *J. Phys. Conf. Ser.* **2019**, *1400*, 066008. [\[CrossRef\]](#)

17. Makeev, S.; Davydov, V.; Rud, V.Y. Features of spectral analysis of nuclear magnetic resonance signal for express-control of hydrocarbon media. *J. Phys. Conf. Ser.* **2021**, *2086*, 012154. [[CrossRef](#)]
18. Davydov, V.; Moroz, A.; Myazin, N.; Makeev, S.; Dudkin, V. Peculiarities of Registration of the Nuclear Magnetic Resonance Spectrum of a Condensed Medium During Express Control of Its State. *Opt. Spectrosc.* **2020**, *128*, 1678–1685. [[CrossRef](#)]
19. Hoult, D. The solution of the Bloch equations in the presence of a varying B1 field—an approach to selective pulse analysis. *J. Magn. Reson.* **1979**, *35*, 69–86. [[CrossRef](#)]
20. Bloch, F. Nuclear induction. *Phys. Rev.* **1946**, *70*, 460. [[CrossRef](#)]
21. McConnell, J. The theory of nuclear magnetic relaxation in liquids. In *The Theory of Nuclear Magnetic Relaxation in Liquids*; Cambridge University Press: Cambridge, UK, 2009.
22. Pedersen, J.B. Theory on transient effects in time resolved ESR spectroscopy. *J. Chem. Phys.* **1973**, *59*, 2656–2667. [[CrossRef](#)]
23. Roberts, J.D. The Bloch equations. How to have fun calculating what happens in NMR experiments with a personal computer. *Concepts Magn. Reson.* **1991**, *3*, 27–45. [[CrossRef](#)]
24. Urquijo, J.; Otálora, J.; Suarez, O. Ferromagnetic resonance of a magnetic particle using the Landau–Lifshitz–Bloch equation. *J. Magn. Magn. Mater.* **2022**, *552*, 169182. [[CrossRef](#)]
25. Pal, R.; Loomba, S. Rogue wave management for the generalized inhomogeneous nonlinear Schrödinger Maxwell–Bloch equation with external potential. *Optik* **2021**, *231*, 166463. [[CrossRef](#)]
26. Yan, Z.; Qu, P.; Xu, B.; Zhang, S.; Ma, J. Solution of two-qubit Rabi model with extended generalized rotating-wave approximation. *Mod. Phys. Lett. B* **2021**, *35*, 2150213. [[CrossRef](#)]
27. Mohamed, A.B.A.; Rahman, A.U.; Eleuch, H. Temporal Quantum Memory and Non-Locality of Two Trapped Ions under the Effect of the Intrinsic Decoherence: Entropic Uncertainty, Trace Norm Nonlocality and Entanglement. *Symmetry* **2022**, *14*, 648. [[CrossRef](#)]
28. Madhu, P.; Kumar, A. Bloch equations revisited: New analytical solutions for the generalized Bloch equations. *Concepts Magn. Reson. Educ. J.* **1997**, *9*, 1–12. [[CrossRef](#)]
29. Zlatanov, K.; Vasilev, G.; Ivanov, P.; Vitanov, N. Exact solution of the Bloch equations for the nonresonant exponential model in the presence of dephasing. *Phys. Rev. A* **2015**, *92*, 043404. [[CrossRef](#)]
30. Grira, S.; Boutabba, N.; Eleuch, H. Atomic population inversion in a two-level atom for shaped and chirped laser pulses: Exact solutions of Bloch equations with dephasing. *Results Phys.* **2021**, *26*, 104419. [[CrossRef](#)]
31. Boutabba, N.; Grira, S.; Eleuch, H. Analysis of a q-deformed hyperbolic short laser pulse in a multi-level atomic system. *Sci. Rep.* **2022**, *12*, 9308. [[CrossRef](#)]
32. Mesgarani, H.; Esmaelzade Aghdam, Y.; Tavakoli, H. Numerical Simulation to Solve Two-Dimensional Temporal-Space Fractional Bloch–Torrey Equation Taken of the Spin Magnetic Moment Diffusion. *Int. J. Appl. Comput. Math.* **2021**, *7*, 1–14. [[CrossRef](#)]
33. Yu, Q.; Turner, I.; Liu, F.; Vegh, V. The application of the distributed-order time fractional Bloch model to magnetic resonance imaging. *Appl. Math. Comput.* **2022**, *427*, 127188. [[CrossRef](#)]
34. Lin, G. General pulsed-field gradient signal attenuation expression based on a fractional integral modified-Bloch equation. *Commun. Nonlinear Sci. Numer. Simul.* **2018**, *63*, 404–420. [[CrossRef](#)]
35. Yin, Y.; Chew, A.; Ren, X.; Li, J.; Wang, Y.; Wu, Y.; Chang, Z. Towards terawatt sub-cycle long-wave infrared pulses via chirped optical parametric amplification and indirect pulse shaping. *Sci. Rep.* **2017**, *7*, 45794. [[CrossRef](#)] [[PubMed](#)]
36. Park, K.J.; Jeong, K.S.; Kim, J.S.; Park, Y.W.; Han, C.g.; Park, J.H. Design of an Antenna High Altitude Electromagnetic Pulse (HEMP) Protection Filter for Tactical Mobile Wireless Communication System. *J. Korean Inst. Electromagn. Eng. Sci.* **2021**, *32*, 446–454. [[CrossRef](#)]
37. Boo, J.; Hammig, M.D.; Jeong, M. Compact lightweight imager of both gamma rays and neutrons based on a pixelated stilbene scintillator coupled to a silicon photomultiplier array. *Sci. Rep.* **2021**, *11*, 3826. [[CrossRef](#)]
38. Genov, G.T.; Hain, M.; Vitanov, N.V.; Halfmann, T. Universal composite pulses for efficient population inversion with an arbitrary excitation profile. *Phys. Rev. A* **2020**, *101*, 013827. [[CrossRef](#)]
39. Blum, K. *Density Matrix Theory and Applications*; Springer Science & Business Media: Berlin/Heidelberg, Germany, 2012; Volume 64.
40. Castin, Y.; Mo, K. Maxwell-Bloch equations: A unified view of nonlinear optics and nonlinear atom optics. *Phys. Rev. A* **1995**, *51*, R3426. [[CrossRef](#)]
41. Boutabba, N.; Grira, S.; Eleuch, H. Atomic population inversion and absorption dispersion-spectra driven by modified double-exponential quotient pulses in a three-level atom. *Results Phys.* **2021**, *24*, 104108. [[CrossRef](#)]
42. Wu, G. Shape properties of pulses described by double exponential function and its modified forms. *IEEE Trans. Electromagn. Compat.* **2014**, *56*, 923–931. [[CrossRef](#)]
43. Boutabba, N.; Eleuch, H. Quantum control of an optically dense atomic medium: Pulse shaping in a v-type three-level system. *Results Phys.* **2020**, *19*, 103421. [[CrossRef](#)]
44. Zhang, J.; Garwood, M.; Park, J.Y. Full analytical solution of the Bloch equation when using a hyperbolic-secant driving function. *Magn. Reson. Med.* **2017**, *77*, 1630–1638. [[CrossRef](#)] [[PubMed](#)]